

Adsorption and Inhibition Analysis of Aconitine and Tubocurarine Alkaloids as Eco-friendly Inhibitors of Pitting Corrosion in ASTM – A47 Low Carbon Steel in HCl Acid Environment

Benedict Ushaka Ugi^{1*}, Mbang Eze Obeten², Victoria Mfon Bassey¹, Louis Hitler¹, Stephen Adie Adalikwu³, Chijioke Everistus Omaliko¹, Desmond Obi Nandi¹, and Ikama Edet Uwah¹

¹Department of Pure & Applied Chemistry, University of Calabar, Calabar, Nigeria

²Department of Chemistry, Cross River State University of Technology, Calabar, Nigeria

³Department of Chemistry, College of Education Akamkpa, Nigeria

* **Corresponding author:**

tel: +234-7067921098

email: ugibenedict@gmail.com

Received: June 9, 2020

Accepted: November 2, 2020

DOI: 10.22146/ijc.56745

Abstract: The research on the adsorption and inhibition analysis of aconitine alkaloid (ACA) and tubocurarine alkaloid (TBA) as eco-friendly inhibitors of pitting corrosion in ASTM – A47 low carbon steel in HCl acid was carried out under the following experimental and analytical methods: gravimetric method, gasometric method, electrochemical impedance spectroscopy, potentiodynamic polarization, and scanning electron microscopy method. Results revealed good inhibitors as inhibition efficiencies were recorded at 98.8% and 91.2% at a maximum inhibitor concentration of 1500 ppm for tubocurarine and aconitine alkaloids, respectively. The inhibition efficiency was found to increase with increasing inhibitor concentrations indicating a strong binding between inhibitor molecules and ASTM – A47 low carbon steel in HCl acid. Electrochemical data strongly supported the efficacy of both inhibitors as earlier presented by the chemical methods as a trend in values of charge transfer resistance, double layer capacitance, corrosion potential, and corrosion current density were in accordance with standards for a good inhibitor. The inhibitors were seen to be spontaneous, stabled, endothermic and physically adsorbed. Adsorption of the inhibitors on metal surface obeyed Langmuir, El-Awady, Freundlich, and Temkin adsorption isotherm as regression values were approximately unity. A monolayer physical adsorption was defined for the system.

Keywords: tubocurarine; aconitine; alkaloids; corrosion; polarization; adsorption; micrographs; Tafel; Nyquist; impedance

■ INTRODUCTION

Corrosion generally is a serious social and economic disadvantage such that millions of dollars have been already spent by different countries in combatting its menace. On a normal day, corrosion can be defined from the instance of deterioration of a material, especially metal, when exposed to an aggressive environment, possible to cause anodic metal dissolution or cathodic hydrogen evolution [1-3]. Corrosion can be electrochemical or dry, depending on the medium of interaction. Disadvantages of corrosion irrespective of types have been long discovered in many areas ranging

from leakages of oil crude at truck pipelines, leakages of food from cans, failure of bridges at different intervals, road accidents from wear and tears of bolts and nuts, the collapse of building in several occasions leading to loss of lives and properties, etc. [2-5]. Pitting corrosion is a localized form of corrosion that involves the formation of cavities and holes in a material (Fig. 1) [1-2,5-6]. For a defect-free perfect material, pitting corrosion could arise from the environment as a factor that may contain aggressive chemical species damaging to the passive film (oxide) hence initiate pitting at oxide breaks [1,4,7].

Ninety-five percent of all uniform corrosion occurs

just after the presence of pitting corrosion, and due to difficulties in early detection of pitting corrosion, it becomes so destructive [3,5-8]. The struggle against corrosion challenges has seen advances from both cathodic protection, anodization, galvanization, surface coating – paint coating, plastic coating, or powder coating, electroplating, and also the use of synthesized inorganic compounds, especially free radicals [4,7-8]. In all these advances, both organic and inorganic corrosion inhibitors have taken the lead in corrosion reduction research in all leading metal-dominant sectors of the economy. The interest in corrosion inhibitors came from their ready availability, non-toxic, eco-friendly nature, and cost-effectiveness, among others [1-3,5-9]. Very interestingly, their ability to adsorb on the metal surface forming protective films, strong ability to combine with corrosion product films to protect the metal surface and formation of precipitates which visibly coat and protect metal surfaces consequence upon the possession of

hetero-compounds and atoms, double bonds, benzene rings, and pie-bond led to usage in testing corrosion inhibition of ASTM – A47 low carbon steel in HCl acid environment [3-9]. Tubocurarine is a benzyloquinoline alkaloid and an active ingredient and naturally occurring curare alkaloid isolated from *Chondrodendron tomentosum* [10]. Meanwhile, aconitine is an alkaloid with a diterpenoid structure that occurs naturally in the roots of *Aconitum napellus* [11]. Structures and chemical formulas of the investigated inhibitors are presented in Fig. 2(a–b).

In line with growing research in the field of organic and eco-friendly corrosion inhibitors as control measures of metal anodic dissolution and cathodic hydrogen evolution, this research was carried out to investigate the adsorption and inhibition analysis of aconitine alkaloid and tubocurarine alkaloid as eco-friendly inhibitors of pitting corrosion in ASTM – A47 Low Carbon Steel in HCl acid.

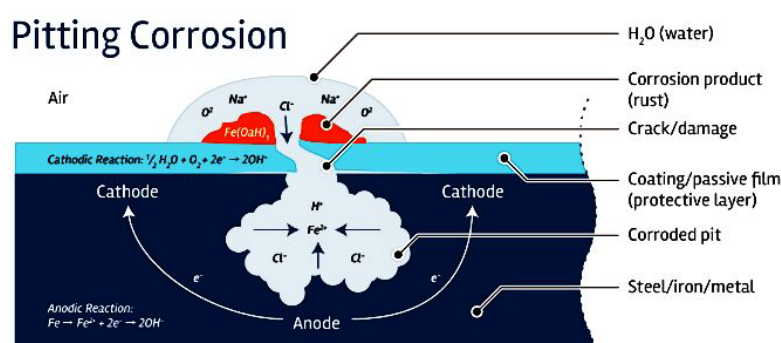


Fig 1. A typical pitting corrosion process

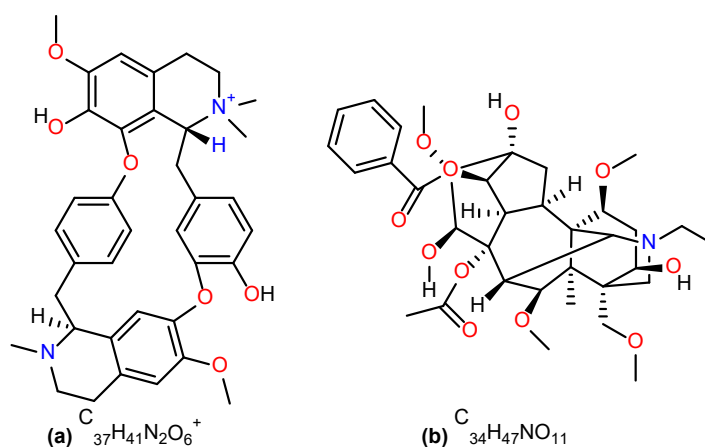


Fig 2. Structure and chemical formula for (a) Tubocurarine and (b) Aconitine alkaloids

■ EXPERIMENTAL SECTION

Materials

The materials used for this research are as follows: *Chondrodendron tomentosum* and *Aconitum napellus* plants, ethanol, diethyl ether, hydrochloric acid, ammonia, hydrobromic acid, tubocurarine alkaloid, tartaric acid, 1000 mL volumetric flask, electronic UNIPOL-820 metallographic polishing machine, ADAM PGW 253e electronic digital weighing balance, distilled water, emery paper, acetone.

Instrumentation

In the course of this research, the following instrumentations used were M36 MEMERY Oven, separating funnel of 500 mL, Soxhlet extraction (heat extraction) process, gravimetric method, gasometric method, electrochemical impedance spectroscopy, potentiodynamic polarization, and scanning electron microscopy.

Procedure

Preparation of stock solution, inhibitors, and metal dressing

The bark of *Chondrodendron tomentosum* and the roots of *Aconitum napellus* plants were both obtained from the bush around the boundary between the Obudu local government area of Cross River State and Tsa Local government area of Benue State, Nigeria. Both plant parts were brought to the Ultra-modern Petroleum Trust Fund Laboratory at the University of Calabar – Nigeria, where they were washed thoroughly to remove sand and other external materials and dried in an M36 MEMERY Oven at 55 °C for 48 h. The dried parts were removed, ground to a powdered form, and sieved to attain a smaller surface area for better surface coverage and optimal extraction. Extraction of 200 g powdered form of the roots and stem separately was carried out using a Soxhlet extractor (heat extraction) for 72 h in ethanol as solvent. The crude ethanol extracts were then evaporated in a water bath for 3.5 h each to concentrate the crude through the removal of retained ethanol to at least one-tenth of the original concentration. In order to isolate each of the alkaloids from the crude extract, a separating funnel of 500 mL was

used. Two hundred mL of 0.5 M HCl was measured into the separating funnel containing 50 g of the crude extract. This was followed immediately by 200 mL diethyl ether to wash and remove resins and fatty materials. The mixture was separated from the non-alkaloids contents while the diethyl ether content was made alkaline (to reduce the acidic content) with excess ammonia and another 150 mL diethyl ether plus 200 mL dilute hydrobromic acid solution to isolate the aconitine alkaloid. For the isolation of tubocurarine alkaloid, tartaric acid was used in place of hydrobromic acid, and the sample was collected in semi-solid form. Seven grams of each alkaloid was weighed into a 1000 mL volumetric flask and digested with 1 M HCl solution, allowed for 24 h for proper absorption and dissolution, then filtered and stored as inhibitors.

Gravimetric method

Gravimetric, or as it is called, weight loss analysis, was carried out on a 5.0 × 1.5 cm diameter low carbon steel every 24 h for 168 h. The resized metals earlier polished mechanically to mirror surface were weighed using ADAM PGW 253e electronic digital weighing balance. They were then immersed into 100 mL beakers containing different concentrations of each inhibitor (300, 500, 750, 1000, 1250, and 1500 ppm) by suspension and allowed for 24 h. After every 24 h, the metals were removed, washed with distilled water, degreased in ethanol, rinsed in acetone, and air-dried, then reweighed to obtain the different loss in weight of metals. The experiment was duplicated and mean taken to allow for accuracy. All reagents were of analytical grade. The corrosion rate of the low carbon steel in both the presence and absence of inhibitors was determined from the slope of the plot of weight loss against time; the surface coverage and inhibition efficiency were obtained from Eq. (1) and (2), respectively.

$$\theta = \frac{Wl_b - Wl_i}{Wl_b} \quad (1)$$

$$IE\% = \frac{Wl_b - Wl_i}{Wl_b} \times 100 \quad (2)$$

where θ is the surface coverage, Wl_b and Wl_i are the weight loss of blank and inhibitor respectively, and IE% is the percentage inhibitor efficiency.

Gasometric method

The gasometric assembly was used for the experiment. Polished resized metals of 2.5×0.05 cm were immersed in different concentrations of each inhibitor (300, 500, 750, 1000, 1250, and 1500 ppm) at different intervals with the initial paraffin oil level properly adjusted to the graduated mark and noted. The conical flask attached to the assembly carrying the metal was let into the water bath and experimental temperature adjusted to 30, 45, 55, and 60 °C, respectively, at different times. After each minute, the fall in the level of paraffin as a result of hydrogen gas evolution was recorded until 60 min. The assembly was stopped, and the experiment restarted for the remaining inhibitor concentrations with new metals. The corrosion rate of the low carbon steel in both the presence and absence of inhibitors was determined from the slope of the plot of weight loss against time; the surface coverage and inhibition efficiency were obtained from Eq. (1) and (2), respectively.

Electrochemical impedance method

The EIS was investigated at ambient temperature in a triple electrode cell compartment using Gamry Reference 600 potentiostat inclusive of a Gamry framework EIS300 system. Echem analyst software was used to analyze the fitting of the data. A saturated calomel (SCE) electrode was introduced as the reference electrode, and a 1 cm² platinum foil was introduced as a counter electrode. The working electrode with dimension 1 × 1 cm was dipped in 1 M HCl acid. Electrochemical tests were conducted within a frequency of 10–10,000 Hz within potentiodynamic conditions, with an amplitude of 5 mV, involving alternating current signals at E_{corr} . All experiments were conducted every 60 min with and without various concentrations of the inhibitors. From the R_{ct} obtained, the retardation efficiency was calculated using Eq. (3):

$$\text{IE\%} = \frac{R_{\text{ct}}^{\text{i}} - R_{\text{ct}}^{\text{o}}}{R_{\text{ct}}^{\text{i}}} \times 100 \quad (3)$$

where R_{ct}^{o} and R_{ct}^{i} represent the charge transfer resistance with and without the inhibitors.

Potentiodynamic polarization method

The potentiodynamic polarization curves were measured at a scan rate of 1 mV s⁻¹, from -500 to 0 mV versus SCE. The Tafel curves for the anode and cathode for low carbon steel dissolution were recorded in both the presence and absence of the inhibitor. Extrapolation of the linear segments of the anodic and cathodic curves gives useful parameters, including anodic and cathodic Tafel slopes, corrosion potential (E_{corr}), and corrosion current density (i_{corr}). The corrosion current density (i_{corr}) was used to calculate the inhibition efficiency of the inhibitors given by Eq. (4):

$$\% \text{IE}_{\text{pdp}} = \left(1 - \frac{I_{\text{corr}}}{I_{\text{corr}}^{\text{o}}} \right) \times 100 \quad (4)$$

Scanning electron microscope analysis

The Scanning electron microscopic study was conducted using the JSM-5600 LV instrument (Hitachi) at the accelerating voltage of 15 kV. For the SEM study, the ASTM – A47 low carbon steel resized metals were allowed to corrode in 1 M HCl solution in the presence and absence of the inhibitors (1 M HCl, 300 ppm, and 1500 ppm). After that, the surfaces of the coupons were examined for their morphological changes.

RESULTS AND DISCUSSION

Gravimetric Analysis/Result

Research findings from the gravimetric experimentation in Table 1 showed increasing inhibition efficiency for both alkaloids (aconitine and tubocurarine) as concentration was increased up to 1500 ppm. This effect has a contrary impact on the corrosion rate of the metal in various concentrations as corrosion rate values were found to be decreasing from 0.934 in 1 M HCl solutions to 0.083 and 0.011 ppm for aconitine and tubocurarine alkaloids, respectively, as earlier observed in a similar work [12-15]. This observation could generally be attributed to the strong binding power, large surface area coverage of both inhibitors on the low carbon steel surface due to adsorption, and significant water molecules substitution at the metal arena [12,16-19]. Comparing inhibition

Table 1. Gravimetric analysis data revealing corrosion rate of metal, surface coverage, and inhibition efficiency of inhibitors on ASTM – A47 low carbon steel in 1 M HCl

Inhibitor Conc. (ppm)	Aconitine alkaloid			Tubocurarine alkaloid		
	Corrosion Rate (mg/cm ² /h)	Surface Coverage	Inhib. Efficiency (%)	Corrosion Rate (mg/cm ² /h)	Surface Coverage	Inhib. Efficiency (%)
1 M HCl	0.934			0.934	-	-
300 ppm + 1 M HCl	0.457	0.51	51.1	0.310	0.67	66.8
500 ppm + 1 M HCl	0.296	0.68	68.3	0.162	0.83	82.6
750 ppm + 1 M HCl	0.205	0.78	78.1	0.095	0.90	89.8
1000 ppm + 1 M HCl	0.158	0.83	83.1	0.029	0.97	96.9
1250 ppm + 1 M HCl	0.110	0.88	88.2	0.022	0.98	97.7
1500 ppm + 1 M HCl	0.083	0.91	91.2	0.011	0.99	98.8

efficiencies of both aconitine and tubocurarine alkaloids, it was observed that low carbon steel was less inhibited in aconitine alkaloids (91.2%) compared to tubocurarine alkaloids (98.8%). This could be due to the presence of more hetero-atoms (2N), pi bonds from double bonds, and benzene rings, including proper orientation of the molecular structure on metal during adsorption [15,20-22].

Gasometric Analysis and Result

To ascertain the effectiveness of the inhibitors when exposed to a relative amount of heat, a gasometric analysis was done, and the data obtained and analyzed are presented in Tables 2 and 3. It was noticed, just as in the case of the gravimetric analysis, inhibition efficiency was found to increase with a corresponding increase in inhibitor concentration. This showed that the inhibitors

Table 2. Gasometric analysis revealing corrosion rate of metal, surface coverage, and inhibition efficiency of tubocurarine on ASTM – A47 low carbon steel in 1 M HCl

Inhibitor Conc. (ppm)	Corrosion Rate (mg/cm ² /h)				Surface coverage				Inhibition efficiency (%)			
	30 °C	45 °C	55 °C	60 °C	30 °C	45 °C	55 °C	60 °C	30 °C	45 °C	55 °C	60 °C
1 M HCl	1.028	1.136	1.771	2.085	-	-	-	-	-	-	-	-
300 ppm	0.254	0.351	0.751	0.968	0.75	0.69	0.58	0.54	75.3	69.1	57.6	53.6
500 ppm	0.200	0.313	0.547	0.753	0.81	0.72	0.69	0.64	80.6	72.4	69.1	63.9
750 ppm	0.169	0.254	0.418	0.594	0.84	0.78	0.76	0.72	83.6	77.6	76.4	71.5
1000 ppm	0.091	0.230	0.376	0.529	0.91	0.80	0.79	0.75	91.2	79.8	78.8	74.6
1250 ppm	0.048	0.205	0.359	0.527	0.95	0.82	0.80	0.75	95.3	82.0	79.7	74.7
1500 ppm	0.016	0.174	0.348	0.501	0.98	0.85	0.80	0.76	98.5	84.7	80.4	76.0

Table 3. Gasometric analysis revealing corrosion rate of metal, surface coverage, and inhibition efficiency of aconitine alkaloid on ASTM – A47 low carbon steel in 1 M HCl

Inhibitor Conc. (ppm)	Corrosion Rate (mg/cm ² /h)				Surface coverage				Inhibition efficiency (%)			
	30 °C	45 °C	55 °C	60 °C	30 °C	45 °C	55 °C	60 °C	30 °C	45 °C	55 °C	60 °C
1 M HCl	1.028	1.136	1.771	2.085	-	-	-	-	-	-	-	-
300 ppm	0.477	0.558	0.887	1.107	0.54	0.51	0.50	0.47	53.6	50.9	49.9	46.9
500 ppm	0.453	0.517	0.835	1.027	0.56	0.54	0.53	0.51	56.0	54.5	52.9	50.7
750 ppm	0.389	0.466	0.786	0.951	0.62	0.59	0.56	0.54	62.2	59.0	55.6	54.4
1000 ppm	0.213	0.382	0.719	0.905	0.79	0.66	0.59	0.57	79.3	66.4	59.4	56.6
1250 ppm	0.174	0.265	0.527	0.658	0.83	0.77	0.70	0.68	83.1	76.7	70.2	68.4
1500 ppm	0.096	0.174	0.386	0.546	0.91	0.85	0.78	0.74	90.7	84.7	78.2	73.8

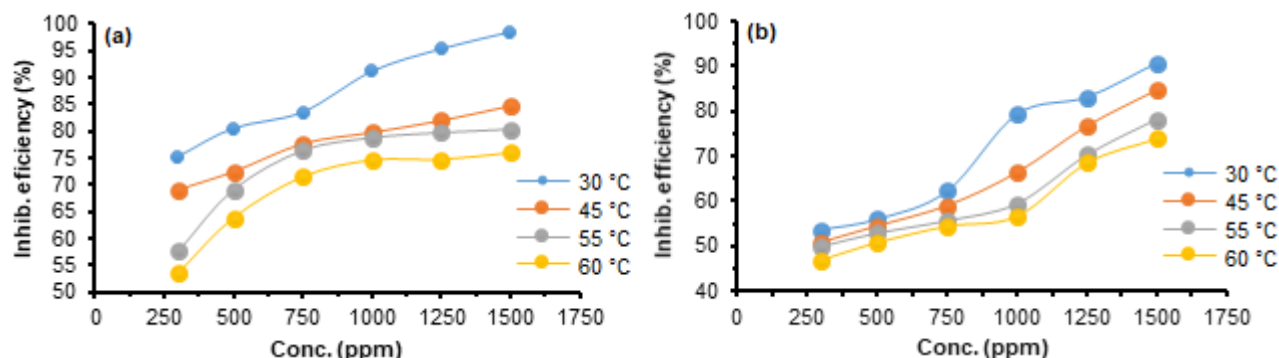


Fig 3. Plots revealing the inhibition efficiency of inhibitors against concentration for (a) tubocurarine and (b) aconitine alkaloids on ASTM – A47 low carbon steel in 1 M HCl

had a good performance on the metal due to proper molecular orientation, size of the inhibitor molecule, and increase adsorption of the inhibitor molecules or its ions on anodic and/or cathodic sites of the low carbon steel Fig. 3(a–b) [17,19,23–28]. However, both inhibitors were seen to be very active in their performance at lower temperatures (30 °C) with an efficiency of 98.5 and 90.7% for tubocurarine and aconitine alkaloids, respectively (Table 2 and 3). In contrary to the result of the corrosion rate of metal at ambient temperature in the gravimetric analysis, the gasometric analysis showed increased corrosion rate and a slight decrease in inhibition efficiency as the temperature was increased accordingly. This is due to the high-temperature effects that bring about agitation and desorption of weakly bounded inhibitor molecules held on the low carbon steel surface by van der Waals forces of attraction rather than ionic bonding [13,22,27–30]. This can also be possible because of the migration of segments of molecules or individual molecules (inhibitors) in jumps, from one place in a site to a vacant hole of the site [17,25,31].

Electrochemical Impedance Spectroscopy

The electrochemical methods allow us to determine the relationship between the ionic, molecular, or charge transfer between the inhibitors and the metal surface in a conducting medium. In this experimental procedure, important information relating to the metal/inhibitor interaction like charge transfer resistance, double layer capacitance, surface coverage, and inhibition efficiency are unraveled. However, data for the double-layer

capacitance for the semicircles and inhibition efficiency were calculated using Eq. (5) and (6).

$$C_{dl} = \frac{1}{\omega Z''} \quad (5)$$

where Z'' is an imaginary component of impedance at any frequency inside the semicircle, and ω is the angular frequency.

$\omega = 2 * \pi * f_{max}$ (in Hz used for measurement of EIS).

Hence,

$$C_{dl} = \frac{1}{2\pi f_{max} Z''} \quad (6)$$

where f_{max} describes the maximum frequency of the semicircle, and the π is 3.142.

However, the data for the IE_R % were obtained from the fitting of the charge transfer resistance values into Eq. (7).

$$IE_R \% = \frac{R_{ct}^0 - R_{ct}^i}{R_{ct}^0} \times 100 \quad (7)$$

Fig. 4(a–b) reveals a Nyquist plot with only one capacitive loop, and this may be due to the presence of just a single charge transfer [17–21,32–35]. It was also observed that the size of the loops increased with the rise of both tubocurarine and aconitine alkaloid concentration up to 1500 ppm, which indicates that both inhibitors were adsorbed on the low carbon steel surface, and the surface area exposed to the 1 M HCl was reduced [14–16,22,36–37]. This was analyzed in Table 4 as the charged transfer resistance values were seen increasing with increasing inhibitor concentration up to 1500 ppm. The double-layer capacitance found decreases with increasing inhibitor concentration, and inhibition efficiency increases

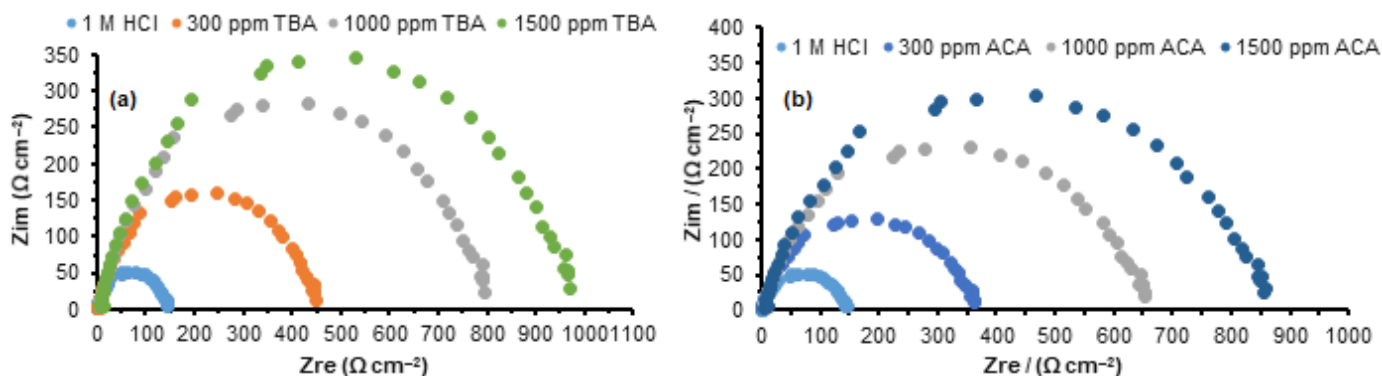


Fig 4. Nyquist plots for the corrosion inhibition of metal by (a) tubocurarine and (b) aconitine alkaloids on ASTM – A47 low carbon steel in 1 M HCl

Table 4. Electrochemical impedance data revealing charge transfer resistance of the metal, double layer capacitance, surface coverage, and inhibition efficiency of inhibitors on ASTM – A47 low carbon steel in 1 M HCl

	Inh. Conc.	R_{ct}	C_{dl}	θ	%IE
TBA	1 M HCl	122	1.3×10^{-5}	-	-
	300 ppm	338	4.7×10^{-6}	0.639	63.9
	1000 ppm	683	2.3×10^{-6}	0.821	82.1
	1500 ppm	923	1.7×10^{-6}	0.868	86.8
ACA	300 ppm	268	5.9×10^{-6}	0.545	54.5
	1000 ppm	674	2.4×10^{-6}	0.819	81.9
	1500 ppm	770	2.1×10^{-6}	0.842	84.2

with the concentration increment. This proved strong adsorption of the inhibitor molecules on the metal surface due to the flow type and flow rate of the inhibitors [28-30,36-40]. It can also be said that the strong adsorption help the system to overcome electron transfer from the positive electrode (anodic site) to the hydrogen ions in the solution phase and subsequent reduction in cathodic hydrogen gas evolution, hence blocking the corrosion reaction [15,27,39-45].

Potentiodynamic Polarization

The corrosion rate is directly proportional to the corrosion current density [33,35]. The plots and values obtained from the potentiodynamic polarization experiment are presented in Table 4. Values are seen to increase with increasing inhibitor concentration, an indication that depicts decreasing diffusion rate for reactants to the surface of the metal and decreasing electrical resistance of metal surface due to strength of bonding to the substrate, cross-linking ability of the inhibitors, and solubility of the 1 M HCl environment [19,24,46-48]. In

addition, as shown in Fig. 5 and Table 5, the addition of tubocurarine and aconitine alkaloid molecules shifted the corrosion potential (E_{corr}) values away from the non-inhibited solution and also showed changes in both the cathodic and anodic polarization branches and values. These results indicate that the added inhibitors acted as mixed-type inhibitors [26-27,39,48-50].

Thermodynamics

Fig. 6 shows plots drawn from the temperature dependence data obtained from the gasometric methods. Values analyzed from the plots of $\ln CR$ against $1/T$, as shown in Table 6.

$$CR = A \exp\left(\frac{-E_a}{RT}\right) \quad (8)$$

By taking the log of Eq. (8), Eq. (9) was obtained.

$$\ln CR = \ln A - \frac{E_a}{RT} \quad (9)$$

where CR is the rate of corrosion, A is the collision constant, R is the universal gas constant, T is the temperature (in kelvin), and E_a is the amount of energy

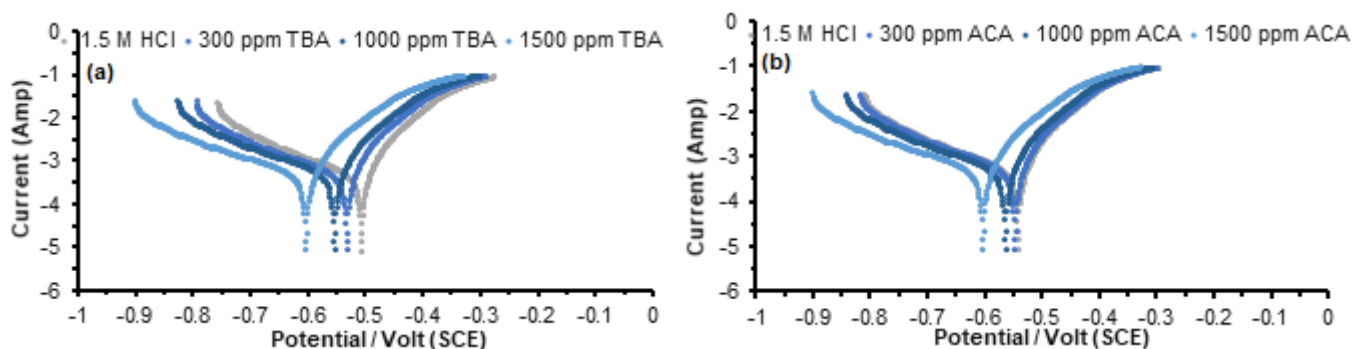


Fig 5. Tafel plots for ASTM – A47 low carbon steel corrosion in 1 M HCl acid solution with and without (a) tubocurarine and (b) aconitine alkaloids

Table 5. Potentiodynamic polarization data revealing corrosion current density, corrosion potential, Tafel slopes, and inhibition efficiency of inhibitors on ASTM – A47 low carbon steel in 1 M HCl

	Inh. Conc.	I_{corr} (mA cm ⁻²)	E_{corr} (mV)	β_c (mV/dec)	β_a (mV/dec)	θ	IE_i (%)
TBA	1 M HCl	2.106	-625	427	550	-	-
	300 ppm	0.847	-419	308	316	0.598	59.8
	1000 ppm	0.414	-295	274	173	0.803	80.3
	1500 ppm	0.269	-174	216	85	0.872	87.2
ACA	300 ppm	0.911	-743	357	319	0.567	56.7
	1000 ppm	0.524	-585	291	236	0.751	75.1
	1500 ppm	0.348	-321	200	170	0.835	83.5

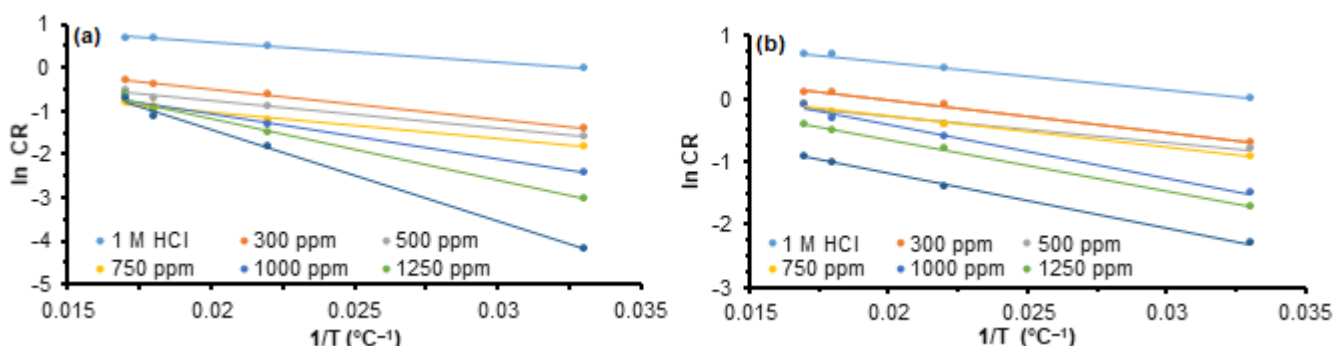


Fig 6. Arrhenius plots revealing the kinetics of corrosion reaction in the presence of (a) tubocurarine and (b) aconitine alkaloids inhibitors on ASTM – A47 low carbon steel in 1 M HCl

required to ensure that a reaction happens [16,19,22,31-37]. The collision coefficient or binding constant derived from Eq. (9) was found to decrease with inhibitor concentration but with a sudden increase from 1250 to 1500 ppm concentration. This is an indication that the inhibitors, especially that of tubocurarine alkaloid, had a stronger binding tendency at higher concentrations. However, activation energy values were seen to be higher in the inhibited solution compared to the non-inhibiting solution (1 M HCl). This is apparently due to the strong

adsorption of molecules of inhibitors onto the ASTM – A47 low carbon steel resized metals and decreasing diffusion rate of corrosion reactants to the metal surfaces, including a possible in situ application advantage consequence to the higher energy barrier required for the corrosion reactants to overcome [20-22,41-43,50-51]. This tendency can also be due to the physical adsorption mechanism of the inhibitor reaction. This has been seen as the activation energy values being less than 20 kJ/mol [15,17-19,42-44,51-53].

Table 6. Thermodynamic data revealing corrosion inhibition of (a) tubocurarine and (b) aconitine alkaloids on ASTM – A47 low carbon steel in 1 M HCl

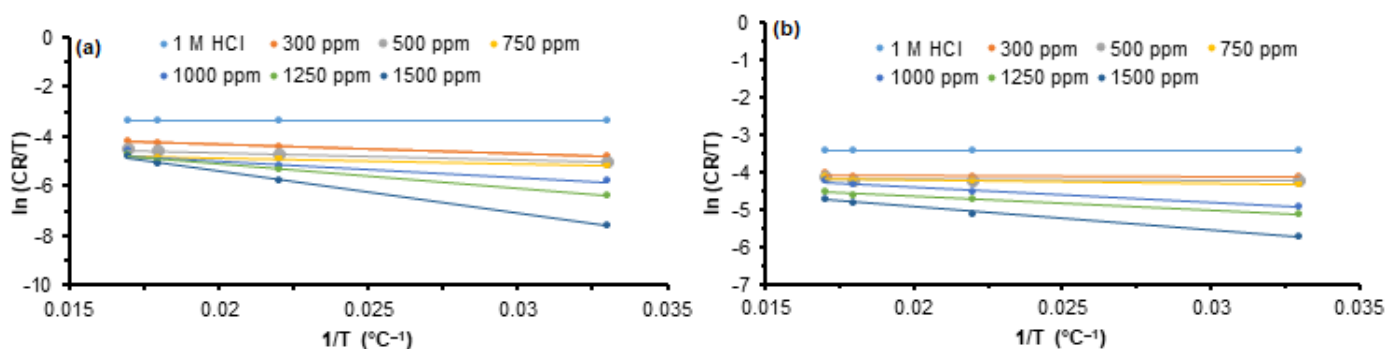
	Inh. Conc.	A	Ea (kJ/mol)	ΔH (kJ/mol)	ΔS (kJ/mol)
Tubocurarine alkaloid	1 M HCl	1.5	3.74	28.267	49.72
	300 ppm	0.9	5.65	29.68	51.14
	500 ppm	0.5	5.39	24.27	45.73
	750 ppm	0.2	5.08	21.94	43.40
	1000 ppm	1.0	8.64	54.22	75.68
	1250 ppm	1.7	11.85	83.55	105.01
	1500 ppm	2.9	17.76	142.27	163.73
Aconitine alkaloid	300 ppm	1.0	4.29	28.40	49.86
	500 ppm	0.6	3.49	28.40	49.86
	750 ppm	0.7	4.02	82.56	104.02
	1000 ppm	1.3	6.99	34.86	56.32
	1250 ppm	1.0	6.71	29.69	51.15
	1500 ppm	0.6	7.23	50.87	72.33

The Eyring transition state equation is given in Eq. (10) was adopted for the graphical determination of both the enthalpy and entropy of adsorption using the gasometric data that evolved from the experimental analysis.

$$\ln \frac{k}{T} = -\frac{\Delta H^\ddagger}{R} \frac{1}{T} + \ln \frac{k_B}{h} + \frac{\Delta S^\ddagger}{R} \quad (10)$$

The values for ΔH^\ddagger and ΔS^\ddagger can be determined from kinetic data obtained from a plot of $\ln \frac{k}{T}$ vs. $\frac{1}{T}$, as seen in Fig. 7(a–b). The straight line with a negative slope, $-\frac{\Delta H^\ddagger}{R}$, and a y-intercept, $\ln \frac{k_B}{h} + \frac{\Delta S^\ddagger}{R}$ from the equation gives the two major thermodynamic parameters investigated. From Table 6, values of the enthalpy of adsorption were seen to be positive, an indication of endothermic reaction in the inhibitor-metal interface and possible absorption of

energy (heat) by the inhibitor reacting system, leading to increase inhibitor reaction and limiting ionic transference at the anodic site of the metal [13-16,29-34,44]. The values were also found to be less than 80 kJ mol⁻¹ claiming that the inhibitors were physically adsorbed on the metal surface [39,43-48]. This is in agreement with the inhibition efficiency result that shows decreasing efficiency while the temperature was increased. The values for the entropy of adsorption, as presented still in Table 6, show that the system was less disordered as values were negative. This situation will allow for the orderly and stable coverage of the inhibitors on the metal surface hence higher activation complex and advancement in the corrosion inhibition reaction [17-25,31,52-54]. The adsorption energy values are presented in Table 6. The values showed that the inhibitors

**Fig 7.** Transition state plots the corrosion inhibition of (a) tubocurarine and (b) aconitine alkaloids on ASTM – A47 low carbon steel in 1 M HCl

presented negative free energy of adsorption, indicating that the inhibitors were stable ones, and their reaction was spontaneous in the forward direction. The inhibitors also influenced the reaction to having the free energy values less negative than 20 kJ mol^{-1} , an indication that the reaction followed a physical adsorption mechanism [19-25,35-39,50,52], and this had been already confirmed from the data obtained for activation energy (E_a) and adsorption enthalpy (ΔH).

Adsorption Evaluation

In an attempt to study the adsorption characteristics of the inhibitor molecules on the metal surface, the Langmuir, El-Awady, Freundlich, and Temkin adsorption isotherms as presented in Fig. 8–11 were studied constructed from Eq. (11), (12), (13), and (14), respectively.

$$\frac{C}{q_e} = \frac{1}{k} + C \quad (11)$$

$$\log\left(\frac{\theta}{1-\theta}\right) = \log b + y \log C \quad (12)$$

$$\ln q_e = \frac{1}{n} \ln C + \ln K_F \quad (13)$$

$$q_e = \frac{RT}{b} \ln C + \frac{RT}{b} \ln K_T \quad (14)$$

where C is the concentration of inhibitors, q_e is the amount of adsorbate adsorbed per unit mass, k is the equilibrium constant, y is the number of inhibitor molecules occupying one active site, b is the heat of sorption, K_T is the equilibrium binding constants and K_F maximum adsorption capacity, while the R and T take their usual meanings.

Generally, it was observed from Table 7–10 that the correlation coefficient values for the isotherms were approximately unity when fitted to the isotherms, and their isotherm equilibrium binding constants were decreasing with temperature. This implies that both

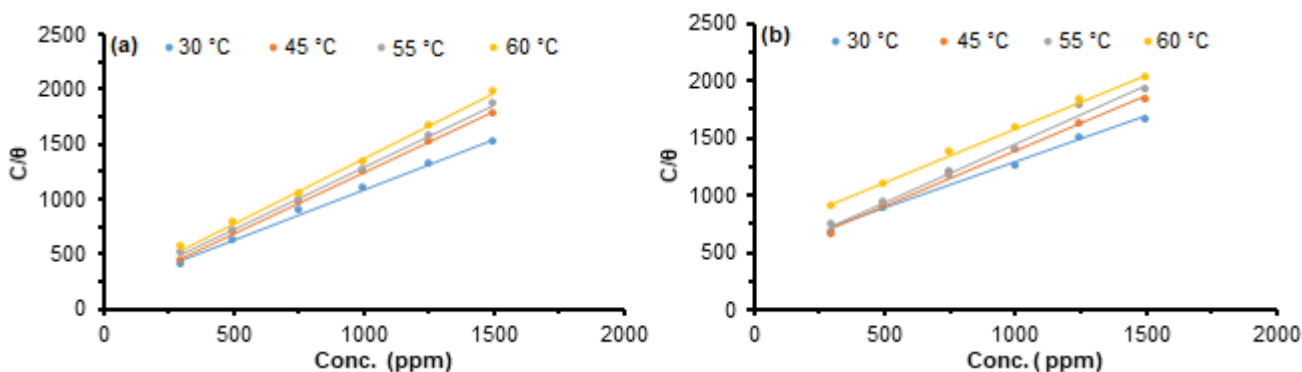


Fig. 8. Langmuir adsorption isotherm plots for (a) tubocurarine and (b) aconitine alkaloids on ASTM – A47 low carbon steel in 1 M HCl

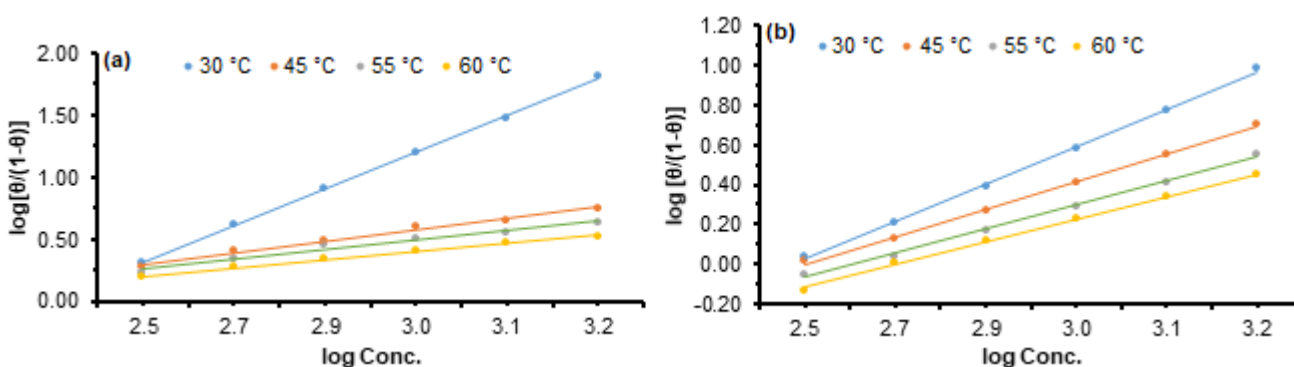


Fig 9. El – Awady adsorption isotherm for (a) tubocurarine and (b) aconitine alkaloids on ASTM – A47 low carbon steel in 1 M HCl

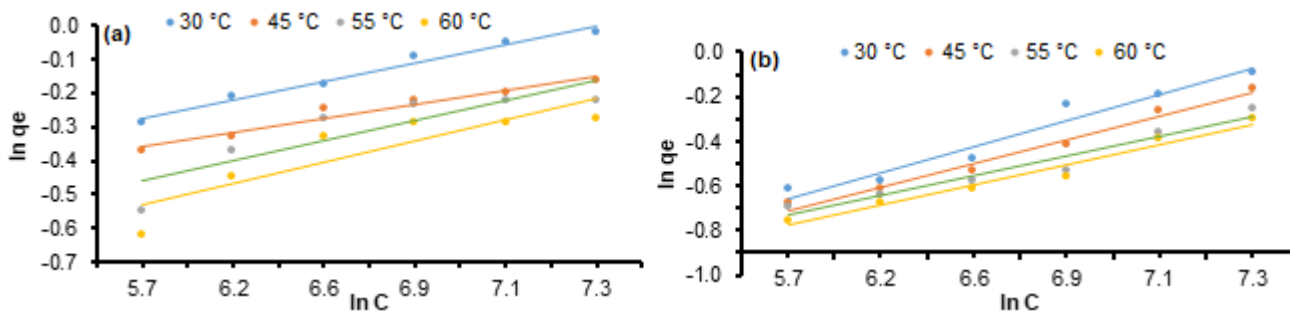


Fig 10. The Freundlich adsorption isotherm showing corrosion inhibition of (a) Tubocurarine and (b) Aconitine alkaloids on ASTM – A47 low carbon steel in 1 M HCl

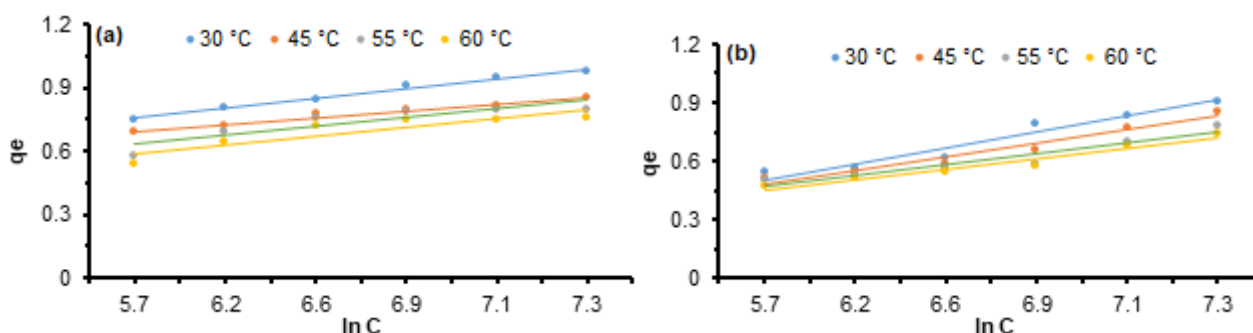


Fig 11. The Temkin adsorption isotherm for (a) tubocurarine and (b) aconitine alkaloids on ASTM – A47 low carbon steel in 1 M HCl

isotherms were obeyed, and a physical adsorption process was eminent [14-18,21-30,39]. However, the Langmuir isotherm was very well obeyed comparatively. The values of k for the Langmuir isotherm were found to be relatively large (> 1) for both inhibitors, an indication that there is

a strong interaction between the inhibitors and the surface and a physical adsorption process [21-29,55]. The El-Awady isotherm characterizes the adsorption sites on the metal surface. The plots in Fig. 9 were obtained from Eq. (12). From the result in Table 8, values

Table 7. Langmuir data for the corrosion inhibition of (a) tubocurarine and (b) aconitine alkaloids on ASTM – A47 low carbon steel in 1 M HCl

Temp. (°C)	Aconitine alkaloid				Tubocurarine alkaloid			
	k	R	slope	ΔG (kJ/mol)	k	R	slope	ΔG (kJ/mol)
30	4.92	0.9713	0.7986	-13.99	1.55	0.9953	0.9272	-11.11
45	4.14	0.9943	0.9712	-13.56	1.22	0.9988	1.1141	-10.51
55	4.26	0.9899	1.0160	-13.63	1.61	0.9987	1.1246	-11.21
60	6.42	0.9980	0.9399	-14.66	1.86	0.9986	1.1814	-11.57

Table 8. El-Awady adsorption data for tubocurarine and aconitine alkaloids on ASTM – A47 low carbon steel in 1 M HCl

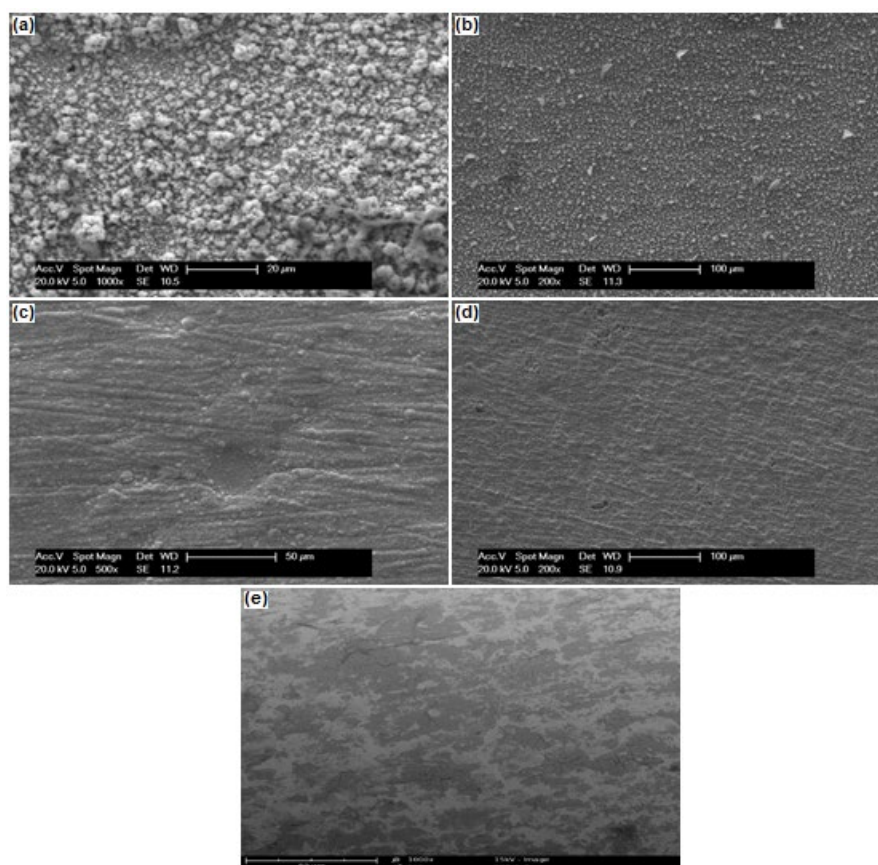
Temp. (°C)	Aconitine alkaloid				Tubocurarine alkaloid			
	1/y	R	y	ΔG (kJ/mol)	1/y	R	y	ΔG (kJ/mol)
30	0.01	0.9996	0.30	-14.69	0.16	0.9985	0.19	-5.45
45	0.20	0.9889	0.09	-9.01	0.13	0.9987	0.14	-7.39
55	0.19	0.9721	0.08	-10.77	0.19	0.9966	0.12	-10.77
60	0.14	0.9915	0.07	10.23	0.22	0.9980	0.11	-12.48

Table 9. Freundlich adsorption isotherm data for tubocurarine and aconitine alkaloids on ASTM – A47 low carbon steel in 1 M HCl

Temp. (°C)	Tubocurarine alkaloid				Aconitine alkaloid			
	K_F	R	1/n	ΔG (kJ/mol)	K_F	R	1/n	ΔG (kJ/mol)
30	0.469	0.9817	0.054	-8.13	0.171	0.9522	0.115	-5.61
45	0.397	0.9588	0.042	-11.6	0.153	0.9812	0.107	-8.00
55	0.301	0.7738	0.055	-12.9	0.151	0.9454	0.089	-9.72
60	0.254	0.7795	0.064	-13.2	0.136	0.9625	0.091	-10.08

Table 10. Temkin adsorption isotherm data for tubocurarine and aconitine alkaloids on ASTM – A47 low carbon steel in 1 M HCl

Temp. (°C)	Tubocurarine alkaloid				Aconitine alkaloid			
	K_T (L/mol)	R	b (kcal/mol)	ΔG (kJ/mol)	K_T (L/mol)	R	b (kcal/mol)	ΔG (kJ/mol)
30	2.21	0.9869	1.1×10^{-5}	-12.00	1.53	0.9512	1.9×10^{-5}	-11.09
45	1.94	0.9669	7.7×10^{-6}	-17.53	1.50	0.9634	1.7×10^{-5}	-16.56
55	1.81	0.7986	1.0×10^{-6}	-21.08	1.52	0.9206	1.3×10^{-5}	-20.29
60	1.73	0.8028	1.0×10^{-6}	-24.68	1.47	0.9424	1.2×10^{-5}	-23.87

**Fig 12.** SEM micrographs of ASTM – A47 low carbon steel in (a) 1 M HCl, (b) 300 ppm ACA, (c) 300 ppm TBA, (d) 1500 ppm ACA and (e) 1500 ppm TBA

of $1/y$ are less than 1, confirming that both inhibitors occupied more than one active site, making them good

inhibitors in 1 M HCl. However, y values were found to decrease with temperature, indicating that the inhibitors

were bounded to the metal surface by weak Van der Waal forces of attraction [39,51-53], and this had been confirmed from the physical adsorption nature of the inhibitors. The $1/n$ value derived from the Freundlich equation serves to describe the linearity of adsorption [54-55]. Normally, when $1/n$ values range from 0.7–10, it implies that the relative adsorption decreases as inhibitor concentration increases and values less than 0.7 implies increased relative adsorption [55-56]. From Table 9, it is observed that the inhibitors proffered increased relative adsorption on the metal surface. It was also observed that the “b” (kcal/mol) values (adsorption energy) in Table 10 were positive and less than unity. This implies an endothermic reaction as already observed with the enthalpy of adsorption (Table 6) and a physical adsorption process, as indicated in the thermodynamic evaluation [54-57].

Surface Morphology

Micrographs drawn from the scanning electron microscopic study are presented in Fig. 12(a-e). A close observation on the slides shows a very rough surface for the metal immersed directly in the 1 M HCl solution. This is an indication of a direct acid attack on the surface, leading to the formation and possible evolution of hydrogen gas, giving rise to corrosion [39,51,29]. It was evident from the micrographs of metals immersed in inhibitor solution that the inhibitor molecules adsorbed strongly on the metal surface, hence blocking all anodic sites from further corrosion as it were with those of the free solution [39,56-60]. However, the micrographs for the inhibition of metal by tubocurarine alkaloid at both inhibitor concentrations (300 ppm and 1500 ppm) presented better adsorption compared to those from aconitine alkaloid, and this confirmed the earlier assertions from other experimental results.

CONCLUSION

The research work presents the following findings. Tubocurarine and aconitine alkaloids inhibited at 98.9 and 91.2%, respectively, in the presence of 1 M HCl, indicating that they are good inhibitors of ASTM – A47 low carbon steel. Temperature dependence of the inhibitors revealed strong adsorption of inhibitors at

lower temperatures, but however, inhibition was found increasing with the concentration of inhibitors at different temperatures. Thermodynamic data presented the inhibitors as stabled, spontaneous, physically adsorbed, and with a little or no degree of disorderliness. Electrochemical results revealed good adsorption performance by the inhibitors as charge transfer resistance was found increasing, double-layer capacitance and polarization resistance were decreasing, and mixed-type inhibition was recorded. Adsorption consideration revealed that both inhibitors occupied more than one active site and as well as obeyed more of the Langmuir adsorption assumptions, hence monolayer. The surface morphology of the metals was smooth enough in both inhibitor concentrations hence strong bonding and large surface coverage.

REFERENCES

- [1] Bardal, E., 2004, *Corrosion and Protection*, Springer-Verlag, London.
- [2] Davis, J.R., 2000, *Corrosion: Understanding the Basics*, ASM International, USA.
- [3] Gergely, A., 2019, *Phenomenal and Theories in Corrosion Science: Methods of Prevention*, Nova Science Publishers Inc., USA.
- [4] McCafferty, E., 2010, *Introduction to Corrosion Science*, Springer-Verlag, New York.
- [5] Ohtsuka, T., Nishikata, A., Sakari, M., and Fushimi, K., 2018, *Electrochemistry for Corrosion Fundamentals*, Springer, Singapore.
- [6] Perez, N., 2016, *Electrochemistry and Corrosion Science*, 2nd Ed., Springer, Cham, Switzerland.
- [7] Rajendran, S., Nguyen, T.A., Kakooei, S., Li, Y., and Yeganeh, M., 2020, *Corrosion Protection of the Nanoscale*, 1st Ed., Elsevier UK.
- [8] Roberge, P.R., 2008, *Corrosion Engineering: Principle and Practices*, McGraw Hill Professional, Canada.
- [9] Talbot, D.E.J., and Talbot, J.D.R., 2018, *Corrosion Science and Technology*, 3rd Ed., CRC Press, Boca Raton, US.
- [10] Tang, W.T., Wong, S.K., Law, T.Y., Pang, K.C., Sin, D., and Tam, Y.K., 2006, Method for the determination of *Aconitum* alkaloids in dietary

- supplements and raw materials by reversed phased liquid chromatography with ultraviolet detection and conformation by tandem mass spectrometry: Single-laboratory validation, *J. AOAC Int.*, 89 (6), 1496–1514.
- [11] Paech, K., and Tracey, M.K., 1955, *Modern Methods of Plant Analysis*, Springer-Verlag, Berlin Heidelberg.
- [12] Akalezi, C.O., and Oguzie, E.E., 2018, Evaluation of anticorrosion properties of *Chrysophyllum albidum* leaves extract for mild steel protection in acidic media, *Int. J. Ind. Chem.*, 7 (1), 81–92.
- [13] Ali, I.H., and Suleiman, M.H.A., 2018, Effects of acid extract of leaves of *Juniperus procera* on corrosion inhibition of carbon steel in HCl solution, *Int. J. Electrochem. Sci.*, 13, 3910–3922.
- [14] Al-Shehri, D.A., 2019, Oil and gas wells: Enhanced wellbore casing integrity management through corrosion rate prediction using an augmented intelligent approach, *Sustainability*, 11 (3), 818.
- [15] Al-Sodani, K.A.A., Al-Amoudi, O.S.B., Maslehuddin, M., and Shameem, M., 2018, Efficiency of corrosion inhibitors in mitigating corrosion of steel under elevated temperature and chloride concentration, *Constr. Build. Mater.*, 163, 97–112.
- [16] Ameh, P.O., and Eddy, N.O., 2018, Experimental and computational chemistry studies on the inhibition efficiency of phthalic acid (PHA) for the corrosion of aluminum in hydrochloric and tetraoxosulphate(VI) acids, *Prot. Met. Phys. Chem. Surf.*, 54 (6), 1169–1181.
- [17] Ammal, P.R., Prajila, M., and Joseph, A., 2018, Effective inhibition of mild steel corrosion in hydrochloric acid using EBIMOT, a 1, 3, 4-oxadiazole derivative bearing a 2-ethylbenzimidazole moiety: Electro analytical, computational and kinetic studies, *Egypt. J. Pet.*, 27 (4), 823–833.
- [18] Bharatiya, U., Gal, P., Agrawal, A., Shah, M., and Sircar, A., 2019, Effect of corrosion on crude oil and natural gas pipeline with emphasis on prevention by ecofriendly corrosion inhibitors: A comprehensive review, *J. Bio-Tribo-Corros.*, 5 (2), 35.
- [19] Boumhara, K., Harhar, H., Tabyaoui, M., Bellaouchou, A., Guenbour, A., and Zarrouk, A., 2019, Corrosion inhibition of mild steel in 0.5 M H₂SO₄ solution by *Artemisia herba-alba* oil, *J. Bio-Tribo-Corros.*, 5 (1), 8.
- [20] Zaher, A., Chaouiki, A., Salghi, R., Boukhraz, A., Bourkhiss, B., and Ouhssine, M., 2020, Inhibition of mild steel corrosion in 1M hydrochloric medium by the methanolic extract of *Ammi visnaga* L. Lam seeds, *Int. J. Corros.*, 2020, 9764206.
- [21] Chaubey, N., Savita, Singh, V.K., and Quraishi, M.A., 2017, Corrosion inhibition performance of different bark extracts on aluminium in alkaline solution, *J. Assoc. Arab Univ. Basic Appl. Sci.*, 22, 38–44.
- [22] Cookey, G.A., Tambari, B.L., and Iboroma, D.S., 2018, Evaluation of corrosion inhibition potentials of green tip forest lily (*Clivia nobilis*) leaves extract on mild steel in acid media, *J. Appl. Sci. Environ. Manage.*, 22 (1), 90–94.
- [23] Dagdag, O., El Harfi, A., Cherkaoui, O., Safi, Z., Wazzan, N., Guo, L., Akpan, E.D., Verma, C., Ebenso, E.E., and Jalgham, R.T.T., 2019, Rheological, electrochemical, surface, DFT and molecular dynamics simulation studies on the anticorrosive properties of new epoxy monomer compound for steel in 1 M HCl solution, *RSC Adv.*, 9 (8), 4454–4462.
- [24] Lavanya, D.K., Priya, F.V., and Vijaya, D.P., 2020, Green approach to corrosion inhibition of mild steel in hydrochloric acid by 1-[morpholin-4-yl(thiophen-2-yl)methyl]thiourea, *J. Fail. Anal. Prev.*, 20 (2), 494–502.
- [25] Es'haghi, M., Amjad, A., Asghari, S., and Lotfi, A., 2018, Studying effect of plantain extract behavior as an eco-friendly corrosion inhibitor on the mild steel in 1 M HCl solution, *Anti-Corros. Methods Mater.*, 65 (3), 310–316
- [26] Essien, E.A., Kavaz, D., Ituen, E.B., and Umoren, S.A., 2018, Synthesis, characterization and anticorrosion property of olive leaves extract-titanium nanoparticles composite, *J. Adhes. Sci. Technol.*, 32 (16), 1773–1794.
- [27] Faiza, M., Zahari, A., Awang, K., and Hussin, H., 2020, Corrosion inhibition on mild steel in 1 M HCl

- solution by *Cryptocarya nigra* extracts and three of its constituents (alkaloids), *RSC Adv.*, 10 (11), 6547–6562.
- [28] Feng, L., Yang, H., Cui, X., Chen, D., and Li, G., 2018, Experimental and theoretical investigation on corrosion inhibitive properties of steel rebar by a newly designed environmentally friendly inhibitor formula, *RSC Adv.*, 8 (12), 6507–6518.
- [29] Fouda, A.S., El-Abbasy, H.M., and El-Sherbini, A.A., 2018, Inhibitive effect of *Artemisia judaica* herbs extract on the corrosion of carbon steel in hydrochloric acid solutions, *Int. J. Corros. Scale Inhib.*, 7 (2), 213–235.
- [30] Go, L.C., Depan, D., Holmes, W.E., Gallo, A., Knierim, K., Bertrand, T., and Hernandez, R., 2020, Kinetic and thermodynamic analyses of the corrosion inhibition of synthetic extracellular polymeric substances, *PeerJ Mater. Sci.*, 2, e4.
- [31] Go, L.C., Holmes, W., and Hernandez, R., 2019, Sweet corrosion inhibition on carbon steel using waste activated sludge extract, *2019 IEEE Green Technologies Conference (GreenTech)*, 3-6 April 2019, Lafayette, LA, USA.
- [32] He, T., Emori, W., Zhang, R.H., Okafor, P.C., Yang, M., and Cheng, C.R., 2019, Detailed characterization of *Phellodendron chinense* Schneid and its application in the corrosion inhibition of carbon steel in acidic media, *Bioelectrochemistry*, 130, 107332.
- [33] Idouhli, R., Koumya, Y., Khadiri, M., Aityoub, A., Abouelfida, A., and Benyaich, A., 2019, Inhibitory effect of *Senecio anteuphorbium* as green corrosion inhibitor for S₃₀₀ steel, *Int. J. Ind. Chem.*, 10 (2), 133–143.
- [34] Wang, Q., Tan, B., Bao, H., Xie, Y., Mou, Y., Li, P., Chen, D., Shi, Y., Li, X., and Yang, W., 2019, Evaluation of *Ficus tikoua* leaves extract as an eco-friendly corrosion inhibitor for carbon steel in HCl media, *Biochemistry*, 128, 49–55.
- [35] Loto, R.T., and Loto, C.A., 2018, Anti-corrosion properties of the symbiotic effect of *Rosmarinus officinalis* and trypsin complex on medium carbon steel, *Results Phys.*, 10, 99–106.
- [36] Majd, M.T., Ramezanzadeh, M., Ramezanzadeh, B., and Bahlakeh, G., 2020, Production of an environmentally stable anti-corrosion film based on *Esfand* seed extract molecules-metal cations: Integrated experimental and computer modeling approaches, *J. Hazard. Mater.*, 382, 121029.
- [37] Ngobiri, N.C., Oguzie, E.E., Oforka, N.C., and Akaranta, O., 2019, Comparative study on the inhibitive effect of Sulfadoxine–Pyrimethamine and an industrial inhibitor on the corrosion of pipeline steel in petroleum pipeline water, *Arabian J. Chem.*, 12 (7), 1024–1034.
- [38] Ngobiri, N.C., and Okorosaye-Orubite, K., 2018, Corrosion pattern of pipeline steel in petroleum pipeline water in the presence of bio-mass derived extracts of *Brassica oleracea* and *Citrus paradise* mesocarp, *Mater. Sci. Appl.*, 9 (1), 216–141.
- [39] Obot, I.B., Umoren, S.A., and Ankah, N.K., 2019, Pyrazine derivatives as green oil field corrosion inhibitors for steel, *J. Mol. Liq.*, 277, 749–761.
- [40] Ogunleye, O.O., Arinkoola, A.O., Eletta, O.A., Agbede, O.O., Osho, Y.A., Morakinyo, A.F., and Hamed, J.O., 2020, Green corrosion inhibition and adsorption characteristics of *Luffa cylindrica* leaf extract on mild steel in hydrochloric acid environment, *Heliyon*, 6 (1), e03205.
- [41] Ahmed, M.H.O., Al-Amiery, A.A., Al-Majedy, Y.K., Kadhum, A.A.H., Mohamad, A.B., and Gaaz, T.S., 2018, Synthesis and characterization of a novel organic corrosion inhibitor for mild steel in 1 M hydrochloric acid, *Results Phys.*, 8, 728–733.
- [42] Othman, N.K., Yahya, S., and Ismail, M.C., 2019, Corrosion inhibition of steel in 3.5% NaCl by rice straw extract, *J. Ind. Eng. Chem.*, 70, 299–310.
- [43] Qiang, Y., Zhang, S., Tan, B., and Chen, S., 2018, Evaluation of *Ginkgo* leaf extract as an eco-friendly corrosion inhibitor of X70 steel in HCl solution, *Corros. Sci.*, 133, 6–16.
- [44] Radwan, A.B., Sliem, M.H., Yusuf, N.S., Alnuaimi, N.A., and Abdullah, A.M., 2019, Enhancing the corrosion resistance of reinforcing steel under aggressive operational conditions using behentrimonium chloride, *Sci. Rep.*, 9 (1), 18115.
- [45] Rodič, P., and Milošev, I., 2019, The influence of additional salts on corrosion inhibition by

- cerium(III) acetate in the protection of AA 7075-T6 in chloride solution, *Corros. Sci.*, 149, 108–122.
- [46] Sangeetha, C., Chinnakani, C., and Selvaraj, S., 2020, *Jatropha gossypifolia* – A green inhibitor act as anticorrosive agent on carbon steel, *J. Adv. Sci. Res.*, 11 (1), 180–186.
- [47] Sanni, O., Popoola, A.P.I., and Fayomi, O.S.I., 2018, Enhanced corrosion resistance of stainless steel type 316 in sulphuric acid solution using eco-friendly waste product, *Results Phys.*, 9, 225–230.
- [48] Shahzad, K., Sliem, M., Shakoor, R.A., Radwan, A.B., Kahraman, R., Umer, M.A., Manzoor, U., and Abdullah, A.M., 2020, Electrochemical and thermodynamic study on the corrosion performance of API X120 steel in 3.5% NaCl solution, *Sci. Rep.*, 10 (1), 4314.
- [49] Singh, D.K., Ebenso, E.E., Singh, M.K., Behera, D., Udayabhanu, G., and John, R.P., 2018, Non-toxic Schiff bases as efficient corrosion inhibitors for mild steel in 1 M HCl: Electrochemical, AFM, FE-SEM and theoretical studies, *J. Mol. Liq.*, 250, 88–99.
- [50] Ikeuba, A.I., Ita, B.I., Okafor, P.C., Ugi, B.U., and Kporokpo, E.B., 2015, Green corrosion inhibitors for mild steel in H₂SO₄ solution: Comparative study of flavonoids extracted from *Gongronema latifolium* with crude extract, *Prot. Met. Phys. Chem.*, 51 (6), 1043–1049.
- [51] Solomon, M.M., Umoren, S.A., Quraishi, M.A., Tripathi, D.B., and Abai, E.J., 2020, Effect of alkyl chain length, flow, and temperature on the corrosion inhibition of carbon steel in a simulated acidizing environment by an imidazoline-based inhibitor, *J. Pet. Sci. Eng.*, 187, 106801.
- [52] Tamalmani, K., and Husin, H., 2020, Review on corrosion inhibitors for oil and gas corrosion issues, *Appl. Sci.*, 10 (10), 3389.
- [53] Tian, H., Li, W., Liu, A., Gao, X., Han, P., Ding, R., Yang, C., and Wang, D., 2018, Controlled delivery of multi-substituted triazole by metal-organic framework for efficient inhibition of mild steel corrosion in neutral chloride solution, *Corros. Sci.*, 131, 1–16.
- [54] Khayyun, T.S., and Mseer, A.H., 2019, Comparison of the experimental results with the Langmuir and Freundlich models for copper removal on limestone adsorbent, *Appl. Water Sci.*, 9 (8), 170.
- [55] Umoren, S.A., and Ebenso, E.E., 2008, Studies of the anti-corrosive effect of *Raphia hookeri* exudate gum-halide mixtures for aluminium corrosion in acidic medium, *Pigm. Resin Technol.*, 37 (3), 173–182.
- [56] Tian, Y., and Zheng, M., 2019, Inhibition effect of silicate and molybdate on the corrosion of SS 316 in neutral corrosive solution at high temperature, *Mater. Res. Express*, 6, 096569.
- [57] Wang, C., Chen, J., Han, J., Wang, C., and Hu, B., 2019, Enhanced corrosion inhibition performance of novel modified polyaspartic acid on carbon steel in HCl solution, *J. Alloys Compd.*, 771, 736–746.
- [58] Wang, X., Jiang, H., Zhang, D., Hou, L., and Zhou, W., 2019, *Solanum lasiocarpum* extract as green corrosion inhibitor for A3 steel in 1 M HCl solution, *Int. J. Electrochem. Sci.*, 14, 1178–1196.
- [59] Zeino, A., Abdulazeez, I., Khaled, M., Jawich, M.W., and Obot, I.B., 2018, Mechanistic study of polyaspartic acid (PASP) as eco-friendly corrosion inhibitor on mild steel in 3% NaCl aerated solution, *J. Mol. Liq.*, 250, 50–62.
- [60] Ugi, B.U., Bassey, V.M., Obeten, M.E., Adalikwu, S.A., and Nandi, D.O., 2020, Secondary plant metabolites of natural product origin-*Strongylodon macrobotrys* as pitting corrosion inhibitors of steel around heavy salt deposits in Gabu, Nigeria, *J. Mater. Sci. Chem. Eng.*, 8 (5), 38–60.